Contents lists available at SciOpen

Food Science and Human Wellness

journal homepage: https://www.sciopen.com/journal/2097-0765

China Food Publishing Co.

Lactiplantibacillus plantarum and quercetin synergistically ameliorate hyperuricemia through targeting multiple pathways

Linyan Zhu, Mengyue Zhang, Juan Cheng, Yixuan Zhang*

School of Life Science and Biopharmaceutics, Shenyang Pharmaceutical University, Shenyang 110016, China

ARTICLE INFO

Article history:
Received 21 December 2023
Received in revised form 28 January 2024
Accepted 8 April 2024

Keywords:
Hyperuricemia
Probiotics
Quercetin
Gut microbiota
Metabolomics

ABSTRACT

Hyperuricemia is a prevalent metabolic disorder resulting from dysregulation of purine metabolism, often accompanied by inflammation. It is characterized by an abnormal elevation in uric acid (UA) levels. In our investigation, the combined treatment with *Lactiplantibacillus plantarum* DY1 and quercetin suppressed the activity of xanthine oxidase and adenosine deaminase, decreased the levels of UA, tumor necrosis factor alpha (TNF-α) and interleukin 1β (IL-β), downregulated gene expression of urate transporter 1 (*URAT1*) and glucose transporter 9 (*GLUT9*), and upregulated organic anion transporter 1 (OAT1) and ATP-binding cassette transporter subfamily G member 2 (ABCG2). The combination increased the abundance of *Lactobacillus* and decreased the abundance of norank_f_norank_o__Clostridia_UCG-014 and *Roseburia.* Metabolomics analysis revealed that the combination of probiotics and quercetin exhibited distinct metabolic pathways compared to their individual administrations. When compared to probiotics alone, the combination led to alterations in glutathione metabolism (oxidized glutathione and glutathione) as well as sphingolipid metabolism (sphingosine and sphinganine). When compared to quercetin alone, the combination resulted in variations in tryptophan metabolism (indole-3-acetamide, 5-hydroxy-*L*-tryptophan, indoleacetaldehyde, 3-(3-indolyl)-2-oxopropanoic acid, 3-indoleacetic acid and 3-methylindole) along with purine metabolism (UA, xanthosine, cyclic adenosine monophosphate (cAMP), adenosine diphosphate (ADP) and adenosine monophosphate (AMP)). The subsequent fecal microbiota transplantation proved that the effect of the combination on reducing UA levels was mediated by the gut microbiota. Therefore, this new combination can be considered a promising adjuvant therapy capable of synergistically alleviating hyperuricemia.

1. Introduction

Hyperuricemia (HUA) is a prevalent clinical disease. When the level of uric acid (UA) in the blood exceeds its saturation point, sodium urate crystals can form in the joints and be deposited in the tissues, leading to local inflammation and tissue damage[1]. The accumulation of these crystals in the kidneys can trigger various renal disorders, such as UA nephropathy[2]. The etiology of HUA can be categorized into three types: excessive production of UA, insufficient excretion type and combination type. The concentration of UA is determined by the equilibrium between dietary purine intake and endogenous synthesis as well as renal excretion of UA in the human body. Moreover, obesity, deficiency in key enzymes involved in purine metabolism, heightened activity of the purine oxidase enzyme system, and genetic factors leading to abnormal expression of urate transporters are also contributory factors to increased UA production or decreased excretion[3]. These factors collectively contribute to the development of HUA.

* Corresponding author at: School of Life Science and Biopharmaceutics, Shenyang Pharmaceutical University, Shenyang 110016, China.
E-mail address: zhangyxzsh@163.com (Y.X. Zhang)
Peer review under responsibility of Beijing Academy of Food Sciences.

SciOpen Publishing services by Tsinghua University Press

http://doi.org/10.26599/FSHW.2024.9250264

In the course of primate evolution, a mutation in the gene encoding uricase hinders humans from metabolizing UA into soluble allantoin, leading to the accumulation of UA[4]. Approximately 1/3 of UA is excreted through the intestinal tract, where gut microbiota can catabolize UA as it traverses both the small and large intestines. The occurrence and progression of HUA are intricately linked to gut microbiota composition. Presently, fecal microbiota transplantation (FMT) technology is extensively employed to validate the therapeutic efficacy of intestinal microbiota manipulation[5]. It should be emphasized that when devising treatment strategies for metabolic disorders, due consideration must be given to the impact exerted by the gut microbiome.

To effectively manage HUA, a comprehensive therapeutic approach involves inhibiting the synthesis and reabsorption of UA, as well as promoting its excretion and decomposition[6]. Currently, clinical interventions primarily rely on xanthine oxidase (XOD) inhibitors like allopurinol to suppress UA production, drugs regulating UA transporters such as probenecid to enhance UA excretion, and UA oxidase medications like rasburicase to convert UA into soluble allantoin. However, the administration of these drugs often results in toxic side effects such as allergic reactions, gastrointestinal disturbances, hepatic impairment and poor patient tolerance. Consequently, there is an urgent need to identify a treatment that can effectively lower UA levels with minimal adverse reactions. Interestingly, the utilization of natural food derived compounds and/or probiotics for treating HUA has garnered increased attention.

Probiotics are defined as a group of living microorganisms that, when consumed in adequate quantities, exert beneficial effects on both humans and animals[7]. A large body of scientific research has unequivocally demonstrated the profound benefits of probiotics, particularly lactic acid bacteria (LAB) in significantly alleviating HUA.

Quercetin, a representative dietary polyphenol, is commonly employed as a prebiotic to enhance the production of probiotics and maintain the equilibrium of the gut microbiota and host health[8]. Previous investigations have demonstrated the potential protective effects of quercetin against HUA[9]. The strategy of harnessing the synergetic effects of probiotics and prebiotics is a promising approach for treating metabolism-related diseases, and this approach has been gaining increasing attention from researchers and clinicians. For instance, the findings of Liu et al.[10] demonstrated the efficacy of combining *Lactobacillus rhamnosus* with inulin for treating colitis in mice. However, due to the complex pathogenesis of HUA, the mechanism of action of probiotics and quercetin remains unclear, especially in terms of the gut microbiome and metabolome. Moreover, the synergistic UA lowering effect of probiotics and prebiotics has not been studied. Therefore, we isolated a probiotic strain named *Lactiplantibacillus plantarum* DY1 from "Duoyi", a traditional fermented food in Yunnan Province, China. This specific strain demonstrates the capability to degrade UA, purine, and nucleoside. We hypothesized that the concomitant use of probiotics with quercetin may inhibit serum UA levels in HUA mice. The potential mechanism of synergistic inhibition of UA accumulation by *L. plantarum* DY1 and its prebiotic quercetin includes perspectives such as UA-related enzymes, UA-related transporter genes, gut microbiota, serum metabolites, and inflammatory response. To the best of our knowledge, this is the first investigation into the UA-lowering activity and underlying mechanisms of the synbiotic composed of *L. plantarum* DY1 and quercetin.

2. Materials and methods

2.1 Reagents and materials

UA (purity ≥ 98%), hypoxanthine (purity ≥ 98%), xanthine (purity ≥ 98%), inosine (purity ≥ 98%) , potassium oxonate (purity ≥ 98%), and XOD were obtained from Shanghai Aladdin Bio-Chem Technology Co., Ltd. (Shanghai, China); allopurinol, quercetin were purchased from Shanghai Sinopharmatic Chemical Reagent Co., Ltd. (Shanghai, China); UA, XOD, and adenosine deaminase (ADA) assay kits were purchased from Nanjing Jiancheng Bioengineering Institute (Nanjing, China); ELISA kits for tumor necrosis factor alpha (TNF-α) and interleukin 1β (IL-β) were purchased from Quanzhou Ruixin Biological Technology Co., Ltd. (Quanzhou, China). Other chemicals are of reagent grade and do not require further handling.

2.2 Strain cultivation

Samples of fermented Duoyi were collected from the market in Lancang County, Pu'er City, Yunnan Province, China. 1 g of fermented Duoyi was weighed and mixed with 10 mL of phosphate buffered saline (PBS) thoroughly. The mixture was then diluted continuously by a tenfold ratio, and the diluents of different gradients were coated on MRS solid medium containing 0.75% $CaCO_3$. The plates were incubated at 37 ℃ for 48 h, and the colonies that formed transparent circles around them were selected for purification. The purified strains were subjected to gram stain and catalase tests, and only the Gram stain-positive and catalase-negative strains were selected. The selected strain was seeded in MRS liquid medium, and a medium containing UA as the sole carbon and nitrogen source was prepared. The strains were cultured in the UA medium. After that, the monoclones were selected and inoculated in MRS liquid medium using an inoculating ring. The pure cultured bacteria were then incubated at 37 ℃ and stored in a 25% glycerol tube[11].

2.3 Determination of in vitro nucleoside degradation activity

The detection method employed in this study was adapted from the work of Lin et al.[12] with subsequent modifications made to enhance its applicability. After centrifugation, the bacterial solution was suspended in sterile saline. The bacterial suspension (1×10^8 CFU/mL) was centrifuged and then resuspended in a 20 mmol/L neutral potassium dihydrogen phosphate (pH 7.0) solution containing 200 μg/mL UA, 200 μg/mL hypoxanthine, 600 μg/mL inosine and 600 μg/mL guanosine, respectively. It was incubated at 37 ℃ for 4 h. The solution was mixed with the terminator perchloric acid at a volume ratio of 9:1 and centrifuged at 4 500 × *g* for 5 min. The supernatant was filtered with a syringe and a 0.22 μm membrane, and then injected into a 1.5 mL vial for determination of UA, hypoxanthine, inosine, and guanosine concentrations by high performance liquid chromatography (HPLC). The degradation rate was calculated using the formula (1):

$$\text{Degradation rate } (\%) = \frac{0.9C - X}{0.9C} \times 100 \quad (1)$$

Where C was initial concentration of UA/hypoxanthine/inosine/guanosine (μg/mL); X was residual concentration of UA/hypoxanthine/inosine/guanosine (μg/mL).

2.4 Determination of hydrophobicity

The value of $OD_{600\,nm}$ of the strain was adjusted to the range of 0.8 using spectrophotometry. The bacterial suspension was mixed with xylene and left at room temperature for 20 min to separate the organic phase from the water phase. Xylene was removed using a pipette, and the absorbance of the bacterial suspension at 600 nm was measured. The hydrophobicity was calculated using the formula (2)[13]:

$$\text{Hydrophobicity}\ (\%) = \frac{A_0 - A_t}{A_0} \times 100 \quad (2)$$

Where A_0 represented the absorbance at 0 h and A_t indicated absorbance at 20 min.

Hydrophobicity was divided into low: 0%−29%, medium: 30%−59%, and high: 60%−100%.

2.5 Autoaggregation test

The bacteria were suspended in sterile PBS, and the absorbance was adjusted to approximately 0.8 at 600 nm. The suspension was incubated at 37 °C for 4 h. The $OD_{600\,nm}$ of the bacterial solution was measured at 0 and 4 h. The autoaggregation was calculated using the formula (3)[14]:

$$\text{Autoaggregation}\ (\%) = (1 - \frac{A_t}{A_0}) \times 100 \quad (3)$$

Where A_0 represented the absorbance at 0 h and A_t indicated the absorbance at 4 h.

2.6 Molecular identification

Genomic DNA was extracted using a bacterial genomic DNA kit. PCR was used to amplify the 16S rRNA gene using primers 27F and 1492R, with DL5000 as the marker. The resulting 16S rRNA sequences were submitted to the GenBank database of NCBI, and blast alignment was conducted to identify sequences with high similarity to the submitted 16S rRNA sequences. The phylogenetic tree was constructed using MEGA 7.0 software.

2.7 Evaluation of the in vitro inhibition of XOD by L. plantarum DY1

To evaluate the inhibitory potential of *L. plantarum* DY1 against XOD, an *in vitro* screening model was employed based on the methodology proposed by Umamaheswari et al.[15] with certain modifications. The bacterial suspension (1×10^9 CFU/mL) was incubated at 37 °C for 16 h, centrifuged, and the supernatant was collected and filtered to obtain cell metabolites. The 1×10^9 CFU/mL bacterial solution was pulse crushed for 10 min under ultrasonic crushing conditions (200 W, work for 5 s, and stop for 5 s), and the cell contents were obtained after filtering the supernatant. 0.75 mL xanthine substrate solution and 0.75 mL bacteria suspension (or intracellular and extracellular liquid) were taken and mixed well. The reaction system had a volume of 2 mL, and the inadequate volume was supplemented with PBS. The experiment was started by adding 0.5 mL of XOD solution (0.5 U/mL), which was held at 25 °C for 20 min in advance. After 30 min, the absorbance at 295 nm was measured for each experimental group. With allopurinol serving as the positive control, the inhibition rate of XOD was calculated using the formula (4):

$$\text{Inhibition rate}\ (\%) = (1 - \frac{C - D}{A - B}) \times 100 \quad (4)$$

Where A represents the absorbance value obtained with XOD in the absence of a sample, B represents the absorbance value obtained without XOD and without a sample, C represents the absorbance value obtained with both XOD and a sample, and D represents the absorbance value obtained with a sample but without XOD.

2.8 Animal experiments

Kunming male mice (SPF, 6 weeks old) were obtained from Hunan Silaike Laboratory Animal Co., Ltd. (SCXK (Xiang) 2019-0004). The animals were kept indoors in a specific pathogen-free (SPF) environment. The feeding conditions included a constant temperature ((23 ± 2) °C) and a relative air humidity of 60%. The light/dark cycle was set at 12 h. In accordance with China's Animal Welfare Law, the use of animals in this study was approved by the Ethics Committee of Jiangxi Agricultural University (approval number: JXAC20180046).

The HUA mouse model was created using modified existing protocols[16-17]. The dosage of probiotics and quercetin is determined based on the findings of our preliminary study. Mice were assigned to 6 groups (n = 9 per group): control group (Control), model group (Model), probiotic group (DY1), quercetin group (Que), combined group (DY1-Que), and positive drug control group (allopurinol, AP). To induce HUA in animals, except for the control group, hypoxanthine (500 mg/kg) and potassium oxonate (250 mg/kg) were administered to the other 5 groups. Blood was collected on 15th day to prepare serum and measure UA levels, and then the experiment continued. On the 16th day, the Model, DY1, DY1-Que and AP groups were given hypoxanthine (500 mg/kg) and potassium oxonate (250 mg/kg). After one hour, *L. plantarum* DY1 suspension (1 mL) at a concentration of 1×10^9 CFU/mL was administered to the DY1 group, quercetin (200 mg/kg) was given to the Que group, *L. plantarum* DY1 suspension (1×10^9 CFU/mL) and quercetin (200 mg/kg) were administered to the DY1-Que group. The AP group was given allopurinol (10 mg/kg). The treatment was administered once a day and lasted 22 days. The feces of mice were collected daily. Thirty minutes after the final dose, mice were anesthetized using sodium pentobarbital, and blood was collected to obtain serum for subsequent analysis. Then, the mice were euthanized and the liver and kidney were taken. The establishment of the HUA model and the specific treatment details were shown in Fig. S1.

2.9 Biochemical index analysis

According to the provided instructions, serum UA and XOD levels were determined, while ADA and XOD concentrations in the supernatant of liver tissues were measured. The tests were conducted following the protocols outlined by the commercial kit manufacturer.

2.10 Histomorphological analysis

The liver and kidney specimens were fixed using a 4% paraformaldehyde solution. Subsequently, the tissues underwent staining with hematoxylin and eosin (H&E), enabling the observation and documentation of their morphological characteristics.

2.11 Real time-polymerase chain reaction (PCR) analysis

Kidney tissues were subjected to total RNA extraction using a tissue extraction kit, following the manufacturer's instructions. The extracted RNA was then reverse transcribed into complementary DNA (cDNA) and amplified accordingly, adhering to the provided protocols. Quantitative PCR analysis was performed as the instructions, with results presented in terms of Ct values. The endogenous control *GAPDH* was normalized and its expression levels were determined using the $2^{-\Delta\Delta Ct}$ method. Specific primer information can be found in Table S1.

2.12 Determination of inflammatory cytokines in kidney tissue

Kidney tissue was homogenized in a 0.9% saline solution, followed by centrifugation at 8 000 × *g* for 10 min to obtain the supernatant. The levels of IL-1β and TNF-α were quantified using ELISA kits.

2.13 Gut microbiota analysis

The total DNA of the fecal gut microbiota was extracted following the protocol provided by the DNA extraction kit. Subsequently, UV spectrophotometry was employed to quantify the extracted DNA. To amplify the V3–V4 region of the 16S rRNA gene, we used primers 338F and 806R. Amplification was conducted using TransStart Fast*Pfu*DNA polymerase, followed by purification of the PCR products. Libraries were constructed utilizing the NEXTFLEX® Rapid DNA-Seq kit. Sequencing was performed on the Illumina MiSeq PE300 platform. The resultant sequences were processed through Trimmomatic for quality control and optimized with Flash (v1.2.11) software. Clustering of the optimized sequences at a 97% similarity threshold was executed using Uparse 7.0, leading to the identification of operational taxonomic units (OTUs). Each sequence was annotated using the RDP classifier, which employs a Bayesian algorithm, and a species abundance table was subsequently generated referencing the Silva database. *α*-Diversity and *β*-diversity analysis were conducted.

2.14 Metabolomics investigation employing liquid chromatography-tandem mass spectrometry (LC-MS/MS)

After being thawed at 4 °C, 100 μL of serum was added to an EP tube. Subsequently, proteins were precipitated using methanol (300 μL), followed by the addition of a 10 μL internal standard (2-chlorophenylalanine). All samples were thoroughly mixed to generate a quality control (QC) sample. The LC-MS analysis was performed using the UHPLC-Q Exactive HF-X system from Thermo Fisher Scientific Inc.. The subsequently acquired data were processed using ProgenesisQI, a metabolomics analysis software developed by Waters Corporation (Milford, USA). Metabolite identification was performed by querying extensive databases, namely the HMDB (https://www.hmdb.ca/) and METLIN (https://metlin.scripps.edu/). The data analysis was performed using the Majorbio cloud platform (https://www.majorbio.com). The data matrices were analyzed using SIMCA 14.1 software, applying principal component analysis (PCA) and orthogonal partial least squares-discriminant analysis (OPLS-DA) to visualize the differences in metabolite profiles among various groups. The metabolites exhibiting statistical significance ($P < 0.05$) and high importance (variable importance in the projection (VIP) > 1) were identified as differential metabolites. Subsequently, an enrichment analysis and investigation of metabolic pathways were conducted using the Kyoto Encyclopedia of Genes and Genomes (KEGG) database search (https://www.genome.jp/kegg/) to gain further insights into their biological functions.

2.15 FMT research

Six-week-old male Kunming mice were divided into two groups: the control (Ctrl) and the antibiotic (Antibiotic). In order to establish a sterile gut model, the mice were administered vancomycin (100 mg/kg), neomycin sulfate (200 mg/kg), metronidazole (200 mg/kg), and ampicillin (200 mg/kg). The antibiotic group received a 7-day course of antibiotics. After discontinuing the antibiotics for 3 days, the mice underwent microbiota transplants via gavage. The mice treated with antibiotics were divided into three groups: Mod, Control (FMT), and DY1-Que (FMT). With the exception to the Ctrl, the remaining three groups were prepared using the previously established method for HUA models. After the natural excretion of feces in the Control group and DY1-Que group in the previous experiment, the fecal samples were promptly collected. Subsequently, 1 mL of PBS was added to each 100 mg of feces, followed by centrifugation at 2 000 × *g* for 4 min. The resulting supernatant served as the transplantation solution. Mice in both the Control (FMT) and DY1-Que (FMT) groups received a dose of 200 μL per mouse of their respective gut microbiota transplantation solution, with a duration of experimentation lasting for 5 weeks. Following a fasting period of 12 h after the final intragastric administration, all mice were anesthetized using 1% pentobarbital sodium for sample collection, including serum and stool samples.

2.16 Statistical analysis

The measurement data were expressed as means ± standard deviation (SD). Data analysis was performed using SPSS 24.0 software (IBM, USA). One-way ANOVA was employed to assess the significance level. $P < 0.05$ indicated statistical significance.

3. Results

3.1 Screening for probiotics with UA degradation ability and high hydrophobicity

The screening of strains was conducted using a medium containing UA as the sole carbon and nitrogen source. Strains DY1, DL2, C13, and D15 exhibited survival capabilities. As depicted in Figs. 1A-D, all four strains demonstrated the ability to degrade UA, hypoxanthine, inosine, and guanosine. Notably, strain DY1 displayed the highest degradation capacity with rates of 93.97% for UA, 87.98% for hypoxanthine, 67.87% for inosine, and 100% for guanosine.

The hydrophobicity analysis presented in Fig. 1E revealed varying levels among the 4 strains towards xylene on their cell surfaces; DY1 exhibited significantly high hydrophobicity (64.05%). Furthermore, Fig. 1F showcased diverse autoaggregation abilities ranging from 26.51% to 60.19%. Remarkably high autoaggregation ability was observed in strain DY1 (60.19%). Consequently, based on these findings, DY1 was selected as the focus of further research endeavors.

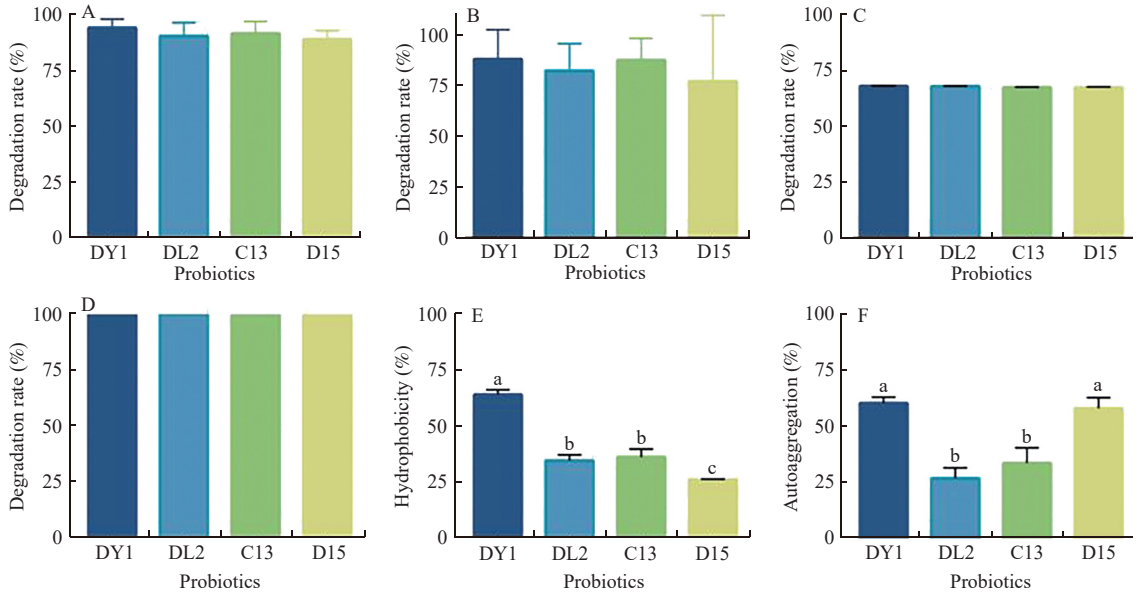

Fig. 1 Degradation rate, hydrophobicity and autoaggregation of strains. (A) UA degradation rate. (B) Hypoxanthine degradation rate. (C) Inosine degradation rate. (D) Guanosine degradation rate. (E) Hydrophobicity of 4 isolates to xylene. (F) Autoaggregation of 4 isolates. Values with different letters represent significant differences ($P < 0.05$). $n = 3$ per group.

3.2 Morphological analysis of strain DY1

According to Fig. S2, strain DY1 exhibited a spherical morphology on MRS agar medium, characterized by a sleek and lustrous surface, intact boundaries, low convexity, viscous consistency, milky white coloration, and opaque colonies. The bacterial cells displayed a rod-shaped structure. Through comprehensive analysis of morphological features and alignment of the 16S rRNA sequence data, the similarity to *L. plantarum* ATCC 14917 was 100%, and strain DY1 was conclusively identified as *L. plantarum* (NCBI accession number OP579101).

3.3 L. plantarum DY1 exhibited a certain degree of XOD inhibitory capability

As depicted in Fig. S3, allopurinol (0.2 mg/mL) exhibited higher sensitivity towards XOD compared to the DY1 bacterial suspension, intracellular substance, and extracellular substance. Upon reaching a reaction time of 30 min, the inhibition rates for allopurinol (0.2 mg/mL), viable bacterial suspension, intracellular extract, and extracellular exudate were found to be 77.85%, 43.07%, 21.53%, and 18.48%, respectively. Both the bacterial suspension and the intracellular extract of this strain exhibited inhibitory activity against XOD, thereby further confirming the significant potential of this strain in reducing UA levels. Moreover, the live bacterial suspension demonstrated significantly higher XOD inhibitory ability compared to both extracellular and intracellular extracts. In conclusion, by establishing an *in vitro* screening model for UA generation, *L. plantarum* DY1 has been proven to possess a certain degree of XOD inhibitory capability. Consequently, *L. plantarum* DY1 holds promising application prospects and value as an XOD inhibitor in daily dietary interventions for the prevention and treatment of HUA.

3.4 L. plantarum DY1, either alone or in conjunction with quercetin, exhibited significant amelioration of HUA

In Fig. 2A, there was no significant difference in serum UA level among all groups. In Fig. 2B, the serum UA concentration of the Model group was significantly enhanced to (215.01 ± 44.04) μmol/L from (128.04 ± 18.53) μmol/L in Control group, indicating the successful establishment of the HUA model ($P < 0.05$). Following a treatment period of 22 days, both UA and XOD levels in HUA mice were significantly higher compared to normal mice ($P < 0.05$). While both DY1 or Que treatments effectively reduced serum UA levels and serum XOD activity compared to the model mice ($P < 0.05$), their effects were weaker than those observed in the DY1-Que group (Figs. 2C-D). In liver tissue, DY1, Que, and DY1-Que groups exhibited significant reductions in XOD and ADA activities compared to Model group (Figs. 2E-F). Preliminarily, it is suggested that *L. plantarum* DY1 and quercetin may potentially reduce UA levels by inhibiting the activity of UA synthetase. However, administration of allopurinol (10 mg/(kg·day)) in mice resulted in liver and kidney damage. Histological examination revealed that renal tubule cells exhibited normal morphology and were fully intact, while the structure of glomeruli appeared clear in Control group. Conversely, HUA mice displayed edema degeneration, enlarged cell size, loose cytoplasm, and an indistinct lumen edge within their renal tubule epithelial cells. Notably, the AP group exhibited evident dilatation of renal tubules along with atrophy and deformation of glomeruli accompanied by infiltration of inflammatory cells (Fig. S4A). These findings suggest a potential renal toxicity associated with allopurinol treatment. The DY1 and Que groups, as well as their combination group, exhibited improved renal tubule morphology and reduced inflammation. The combination group demonstrated the least degree of kidney injury. Compared to Control group, hepatocytes in Model group exhibited lipid vacuoles and localized necrosis. Following treatment, lipovacuolar degeneration of

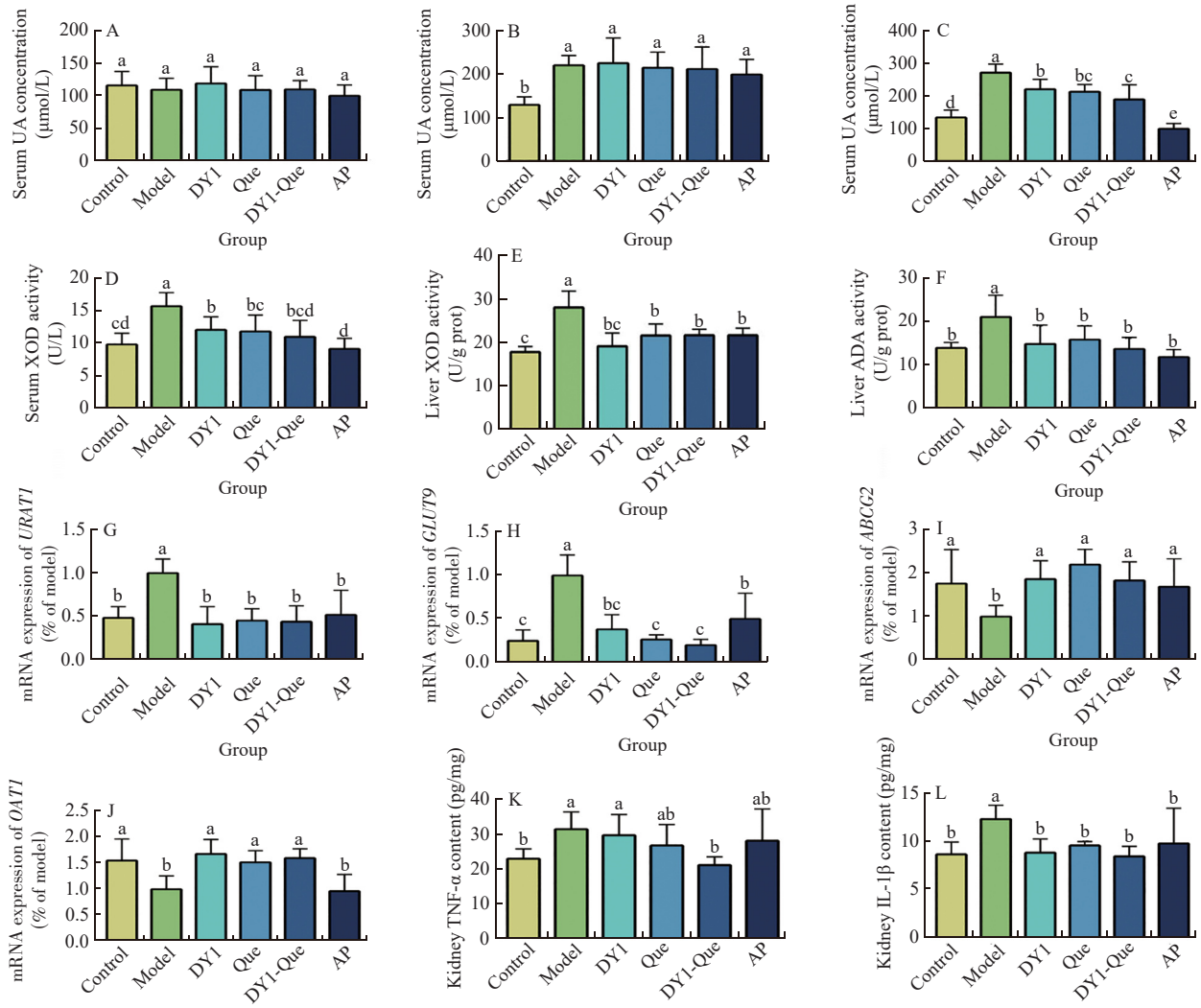

Fig. 2 Biochemical markers, mRNA levels and inflammatory cytokine levels in mice. Serum UA concentration in 0 day (A), 15 days (B), 37 days (C). Serum XOD activity (D), liver ADA activity (E), liver XOD activity (F) in 37 days. The mRNA levels of *URAT1* (G), *GLUT9* (H), *ABCG2* (I), *OAT1* (J). Kidney TNF-α content (K), IL-1β content (L). Values with different letters represent significant differences ($P < 0.05$). (A-E) $n = 6–9$ per group; (F-L) $n = 5–6$ per group.

hepatocytes was mitigated across all groups. These findings suggest that probiotics and quercetin possess hepatoprotective effects. Among them, the combination group had the best liver protection effect (Fig. S4B).

3.5 Effect of L. plantarum DY1 and quercetin on the expression of urate transporter genes

Two types of proteins involved in the reabsorption of UA (urate transporter 1 (URAT1) and glucose transporter 9 (GLUT9)) and two types of proteins involved in the secretion of UA (organic anion transporter 1 (OAT1) and ATP-binding cassette transporter subfamily G member 2 (ABCG2)) were utilized to investigate the capacity for UA excretion. The results demonstrated a significant increase in the expression levels of *URAT1* and *GLUT9* genes in HUA mice ($P < 0.05$). Following administration of the AP, DY1, Que, and DY1-Que groups, there was a downregulation observed in the mRNA expression of *URAT1* and *GLUT9* ($P < 0.05$). In comparison to the control group, a notable decrease was found in the expressions of *ABCG2* and *OAT1* genes in HUA mice ($P < 0.05$). Treatment with DY1, Que, and DY1-Que significantly upregulated mRNA levels of the *ABCG2* and *OAT1*. Allopurinol exhibited a significant upregulation effect on the expression of *ABCG2* but not *OAT1* (Figs. 2G-J). These findings suggest that probiotic *L. plantarum* DY1 combined with quercetin promotes UA excretion by down-regulating *URAT1* and *GLUT9* expressions while up-regulating *ABCG2* and *OAT1* expressions. Notably, synergistic treatment with *L. plantarum* DY1 and quercetin resulted in the most pronounced suppression of *GLUT9* mRNA expression.

3.6 Effect of L. plantarum DY1 and quercetin on proinflammatory cytokines

To further elucidate the underlying mechanism by which *L. plantarum* DY1 and quercetin lower UA levels, the renal inflammatory response was assessed by measuring IL-1β and TNF-α levels (Figs. 2K and L). The results revealed a significant elevation in IL-1β and TNF-α levels in HUA mice ($P < 0.05$). However, following administration of allopurinol, *L. plantarum* DY1, quercetin, or a combination of *L. plantarum* DY1 and quercetin, there was a notable

reduction in IL-1β levels ($P < 0.05$). Interestingly, only the combination of *L. plantarum* DY1 and quercetin exhibited a significant reversal of TNF-α level. These findings suggest that one potential mechanism through which the *L. plantarum* DY1 and quercetin combination reduces UA is via inhibition of inflammation.

3.7 *L. plantarum DY1 and quercetin exerted an impact on the gut microbiota*

The 16S rRNA sequencing method was employed to quantify the abundance of microflora across diverse taxonomic hierarchies. A total of 1 402 873 optimized sequences were obtained from 30 fecal samples in this experimental study. Rarefaction curves were employed to elucidate species richness and community evenness. As the amount of sequencing data increased, the number of OTUs gradually rose, and the rarefaction curves exhibited a tendency to plateau, indicating sufficient sequencing coverage was achieved. The *α*-diversity analysis revealed significantly enhanced Shannon and Chao indexes in the HUA mice model compared to other groups, suggesting greater diversity and abundance of gut microbiota (Fig. S5).

The *β*-diversity was utilized to elucidate the structure and functionality of the gut microbiota. Unweighted UniFrac based PCA and principal coordinate analysis (PCoA) exhibited significant differentiation between the model group and normal mice, indicating a disturbance in the gut microbiota composition of HUA mice (Figs. 3A-B). Adonis analysis was used to detect differences between groups. Therefore, despite no clear trend of separation between groups being evident in the PCA and PCoA, the outcomes of the adonis statistical test were able to detect substantial disparities in flora composition across different groups (Table S1). Stratified clustering

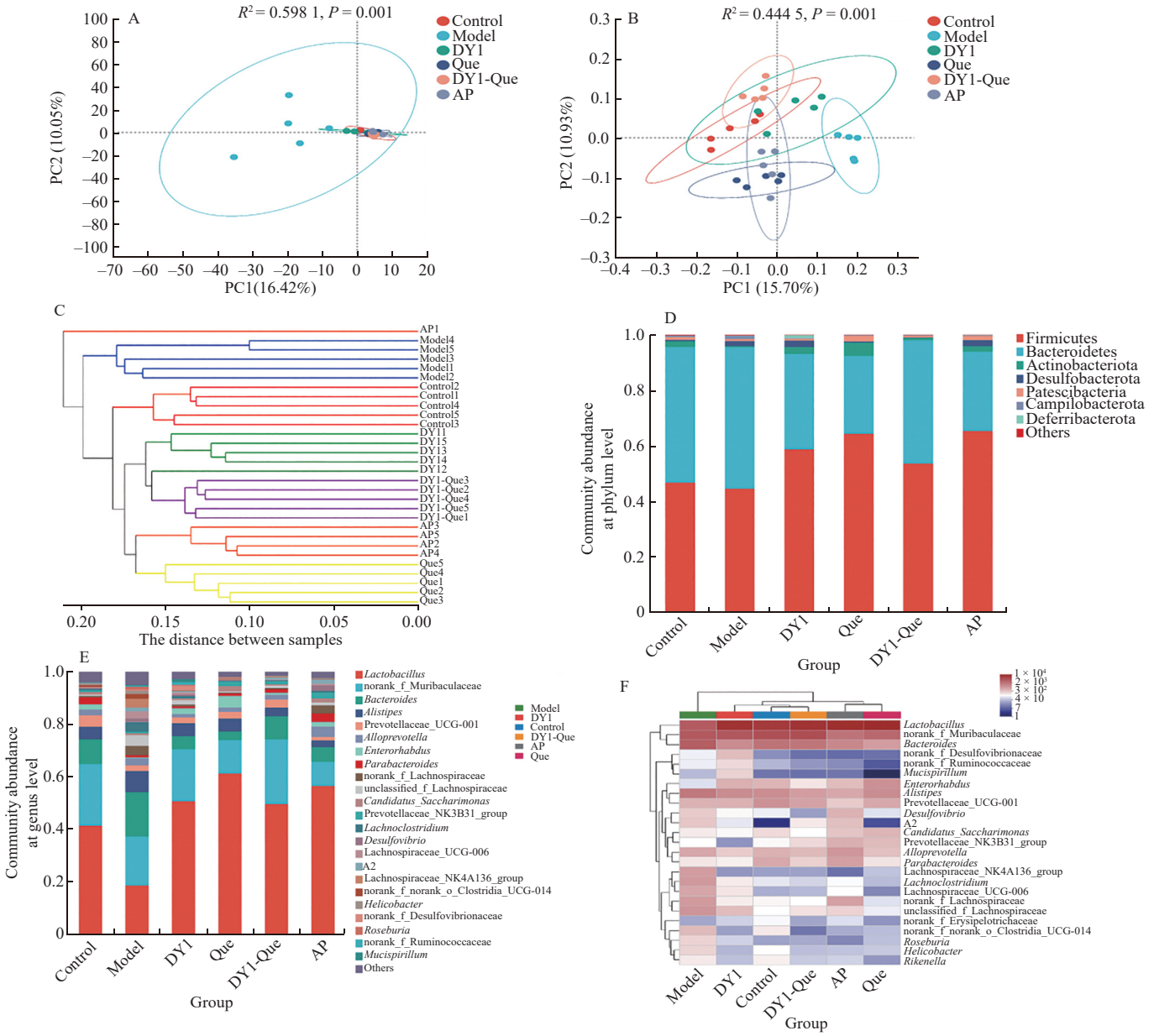

Fig. 3 Gut microbiota analysis. (A) PCA. (B) PCoA. (C) Hierarchical clustering based on unweighted UniFrac. (D) Phylum level community composition. (E) Genus level community composition. (F) Heatmap of the top 25 gut microbiotas at the genus level. $n = 5$ per group.

results were consistent with those obtained from PCA and PCoA (Fig. 3C). These findings provide compelling evidence that combined treatment with *L. plantarum* DY1 and quercetin can profoundly impact the composition of the gut microbiota in HUA mice. There was relatively minimal separation observed between the Control and DY1-Que groups.

To elucidate the potential microorganisms influencing UA metabolism regulation, a thorough analysis was conducted to examine the distribution of the microbial community across different taxonomic levels. The community histogram effectively illustrates the dominant communities and their respective abundances in each sample, with particular emphasis on those exceeding 1%. At the phylum level, Firmicutes, Bacteroidetes, Actinobacteriota, Desulfobacterota, Patescibacteria, Campilobacterota, and Deferribacterota emerged as the predominant communities (Fig. 3D). Notably depicted in Figs. 4A-B is a reduction in Firmicutes abundance alongside an increase in Bacteroidetes abundance among HUA mice. The decreasing trend in Firmicutes abundance and the increasing trend in Bacteroidetes abundance were effectively mitigated across all treatment groups. Compared to HUA mice, the administration of quercetin and allopurinol significantly restored Firmicutes abundance while significantly reducing Bacteroidetes abundance ($P < 0.05$). The administration of quercetin also significantly increased the abundance of Patescibacteria ($P < 0.05$) (Fig. 4C). In HUA mice, there was a significant decrease in the abundance of Actinobacteriota compared to control mice ($P < 0.05$). The administration of *L. plantarum* DY1 alone or in combination with quercetin resulted in an increase in the abundance of Actinobacteriota. Specifically, *L. plantarum* DY1 had a significant impact on the abundance of Actinobacteriota ($P < 0.05$) (Fig. 4D). Subsequently, the distribution of microbial genera within each group was analyzed. The major microbial communities identified in mouse intestinal contents were *Lactobacillus*, norank_f__Muribaculaceae, *Bacteroides*, *Alistipes*, and Prevotellaceae_UCG-001 (Figs. 3E-F).

As the dominant community, the abundance of *Lactobacillus* was 41.13% in the Control, 18.23% in the Model, 50.48% in the DY1, 61.05% in the Que, 49.43% in the DY1-Que, and 56.35% in the AP. There was a statistically significant reduction ($P < 0.05$) in the abundance of *Lactobacillus* among mice with HUA compared to control mice, however, administration across all groups led to a significant increase ($P < 0.05$) in *Lactobacillus* abundance (Fig. 4E).

An increased abundance of Lachnospiraceae_UCG-006 and *Roseburia,* as well as a decreased abundance of *Enterorhabdus* and *Parabacteroides*, were observed in HUA mice. Importantly, the administration of *L. plantarum* DY1 significantly augmented the abundance of *Enterorhabdus* ($P < 0.05$). The administration of allopurinol notably enhanced the abundance of *Enterorhabdus* and *Parabacteroide*s ($P < 0.05$). Conversely, quercetin administration exhibited a significant reduction in the abundance of Lachnospiraceae_UCG-006 ($P < 0.05$). Compared to the HUA mice, there were significant alterations in the abundance of norank_f__Lachnospiraceae, *Candidatus_Saccharimonas*, norank_f__norank_o__Clostridia_UCG-014, and Prevotellaceae_NK3B31_group in the different treatment groups ($P < 0.05$). However, when compared to normal mice, these microbial communities did not exhibit significant changes in the model group. Notably, compared to Model group, a noteworthy reduction was observed in the levels of *Roseburia* across all treatment groups ($P < 0.05$). Moreover, the combination of *L. plantarum* DY1 and quercetin led to a more pronounced decline in the abundance of *Roseburia* (Figs. 4E-M).

It is noteworthy that the combination of *L. plantarum* DY1 and quercetin supplementation effectively ameliorated dysregulation in the gut microbiome, thereby indicating a synergistic impact resulting from their combination. A correlation analysis was performed to explore the association between biochemical markers and dominant gut microbiota. As depicted in Fig. S6, there was a negative correlation between *Lactobacillus* and *Parabacteroides* with XOD and UA ($P < 0.05$), while *Roseburia* showed a positive correlation with XOD and UA ($P < 0.05$). These findings suggest that the combined administration of *L. plantarum* DY1 and quercetin synergistically modulated the composition and structure of the gut microbiota, thereby aiding in regulating UA levels.

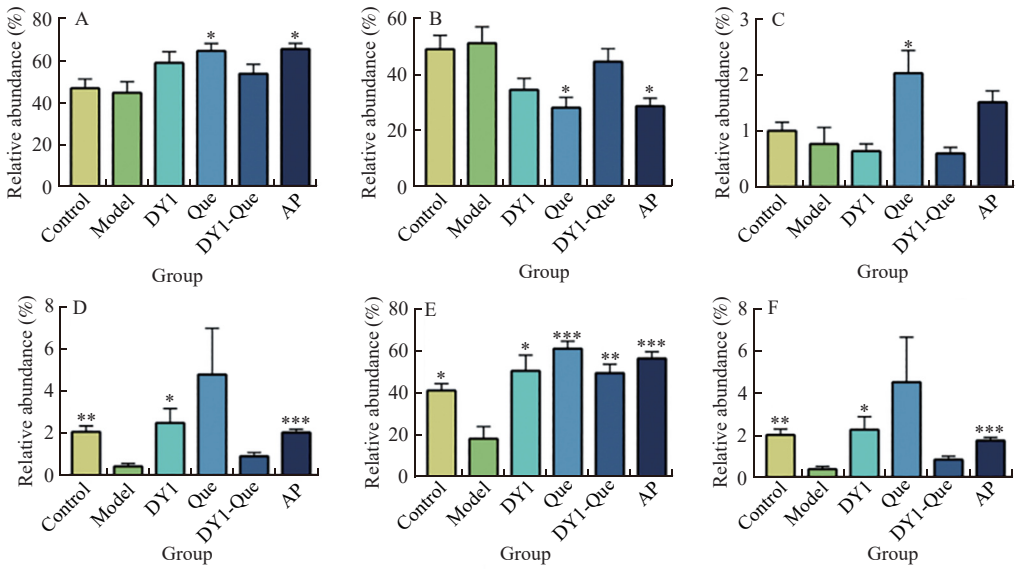

Fig. 4 Gut microbiota composition of mice. (A-D) Phylum level multigroup comparison. (A) Firmicutes, (B) Bacteroidetes, (C) Patescibacteria, (D) Actinobacteriota. (E-M) Genus level multigroup comparison. (E) *Lactobacillus*, (F) *Enterorhabdus*, (G) *Parabacteroides*, (H) norank_f__Lachnospiraceae, (I) *Candidatus_Saccharimonas*, (J) Prevotellaceae_NK3B31_group, (K) Lachnospiraceae_UCG-006, (L) norank_f__norank_o__Clostridia_UCG-014, (M) *Roseburia*. Statistical analysis was followed by Welch's *t* test. *$P < 0.05$; **$P < 0.01$; ***$P < 0.001$, vs the Model group. $n = 5$ per group.

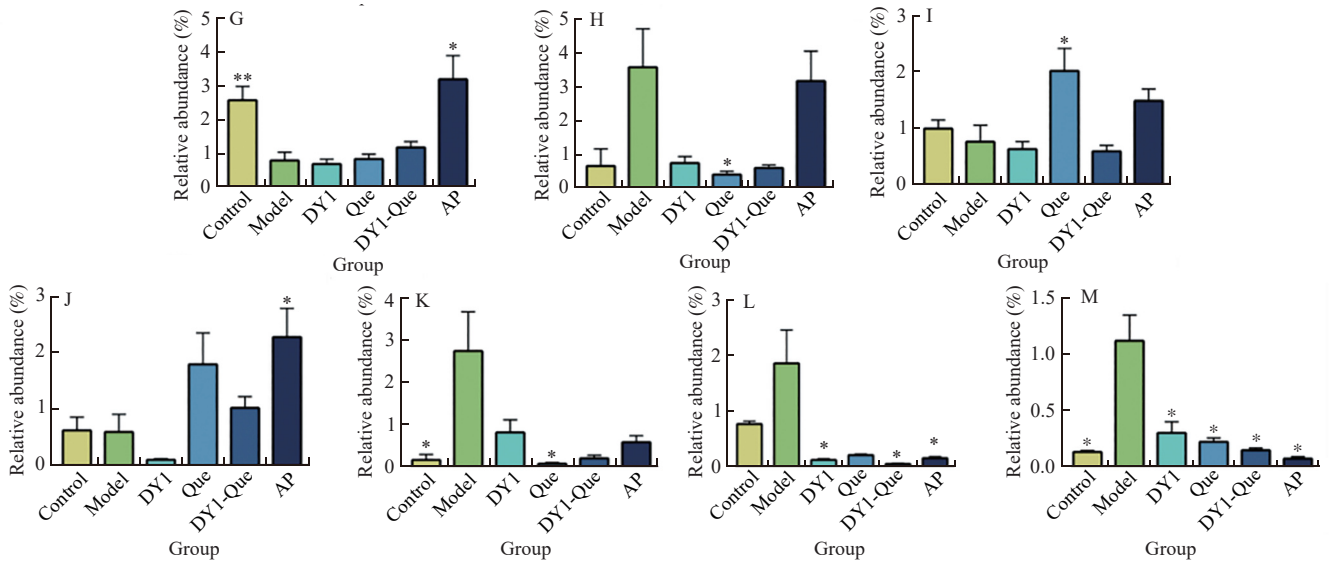

Fig. 4 (*Continued*)

3.8 Metabonomics analysis

Non-targeted metabolomics techniques were used to screen for potential differential metabolites involved in the regulation of HUA by *L. plantarum* DY1 and quercetin. The positive ion and negative ion current diagrams exhibited satisfactory peak shapes and a more uniform distribution under the experimental conditions (Fig. S7).

As depicted in the PCA diagram (Figs. 5A-B), both in positive and negative modes, model mice were distinctly separated from the other groups, while the metabolic profiles of the AP and the DY1-Que exhibited closer resemblance to those of normal mice. In Figs. 5C-D, an OPLS-DA model was employed to discern differential metabolites between Control and Model groups. The selection of differential metabolites was based on VIP > 1 and $P < 0.05$.

A total of 155 differential metabolites were identified in the Model group, which are potentially involved in the pathogenesis of HUA mice. Similarly, compared to the Model, there were 61, 88, 169, and 192 differential metabolites found in the DY1, Que, DY1-Que, and AP groups, respectively. Twenty-one cross-metabolites were identified by overlapping the differential metabolites between the Model vs the Control and between the DY1 vs the Model (Fig. 5E). Similarly, in the Que, DY1-Que and AP groups, there were 22, 105 and 106 overlapping differential metabolites observed, respectively (Figs. 5F-H). Among these 155 metabolites, 124 could be successfully annotated using the HMDB, METLIN or KEGG databases. These metabolites were considered as significantly differential metabolites for HUA. Among them, 16, 18, 83, and 88 significantly differential metabolites associated with HUA mice in the DY1, Que, DY1-Que, and AP groups respectively exhibited alterations. The specific changes are presented in Table S2. As depicted in Fig. S8, the heatmap visually illustrated the relative abundance of the top 50 significantly differential metabolites across 6 groups. We observed a significant overlap between the differential metabolites in the DY1-Que group and those in the Control group, indicating a similar composition to that of differential metabolites found in the normal mice. These findings suggest distinct regulatory effects on serum metabolites in HUA mice by different therapeutic drugs. The combination of *L. plantarum* DY1 and quercetin resulted in more alterations of differential metabolites compared to either treatment alone, thereby exhibiting an enhanced effect on alleviating metabolic disorders associated with HUA.

KEGG enrichment and topological analyses were used to evaluate the role of metabolites in biological reactions by examining their positions in relevant pathways and to identify the specific metabolic pathways involved.

The pathway enrichment analysis was carried out on 124 different metabolites in the Control group and Model group. Ultimately, it was found that HUA disrupted 10 metabolic pathways (Fig. S9). As depicted in Figs. 5I-L, a total of 16 metabolites exhibited pathway enrichment between Model vs Control and DY1 vs Model. Two crucial metabolic pathways, namely purine metabolism and tryptophan metabolism, were identified as the most significant (impact > 0, $P < 0.05$). Moreover, a total of 18 metabolites exhibited pathway enrichment between Model vs Control and Que vs Model. Notably, four distinct metabolic pathways were recognized: glutathione metabolism, galactose metabolism, sphingolipid metabolism, and phenylalanine, tyrosine and tryptophan biosynthesis (impact > 0, $P < 0.05$). Through pathway enrichment analysis, it was determined that DY1-Que predominantly pertains to glutathione metabolism, sphingolipid metabolism, tryptophan metabolism and purine metabolism (impact > 0, $P < 0.05$). The differential metabolites included oxidized glutathione, indoleacetaldehyde, cyclic adenosine monophosphate (cAMP), sphingosine, sphinganine, indole-3-acetamide, 3-(3-indolyl)-2-oxopropanoic acid, 3-indoleacetic acid, UA, 5-hydroxy-*L*-tryptophan, xanthosine, 3-methylindole, adenosine diphosphate (ADP), adenosine monophosphate (AMP) and glutathione. These 15 differential metabolites could be regarded as biomarkers for the combination treatment group, and their clustering heatmap in all groups were shown in Fig. S10A. As shown in Fig. S10B, tryptophan metabolism and purine metabolism accounted for a large proportion. A total of 88 cross-metabolites were compared between the Model vs Control and AP vs Model groups, leading to the identification of seven metabolic pathways: glutathione metabolism, sphingolipid metabolism, tryptophan metabolism, pantothenate and CoA biosynthesis, purine metabolism, caffeine metabolism, and

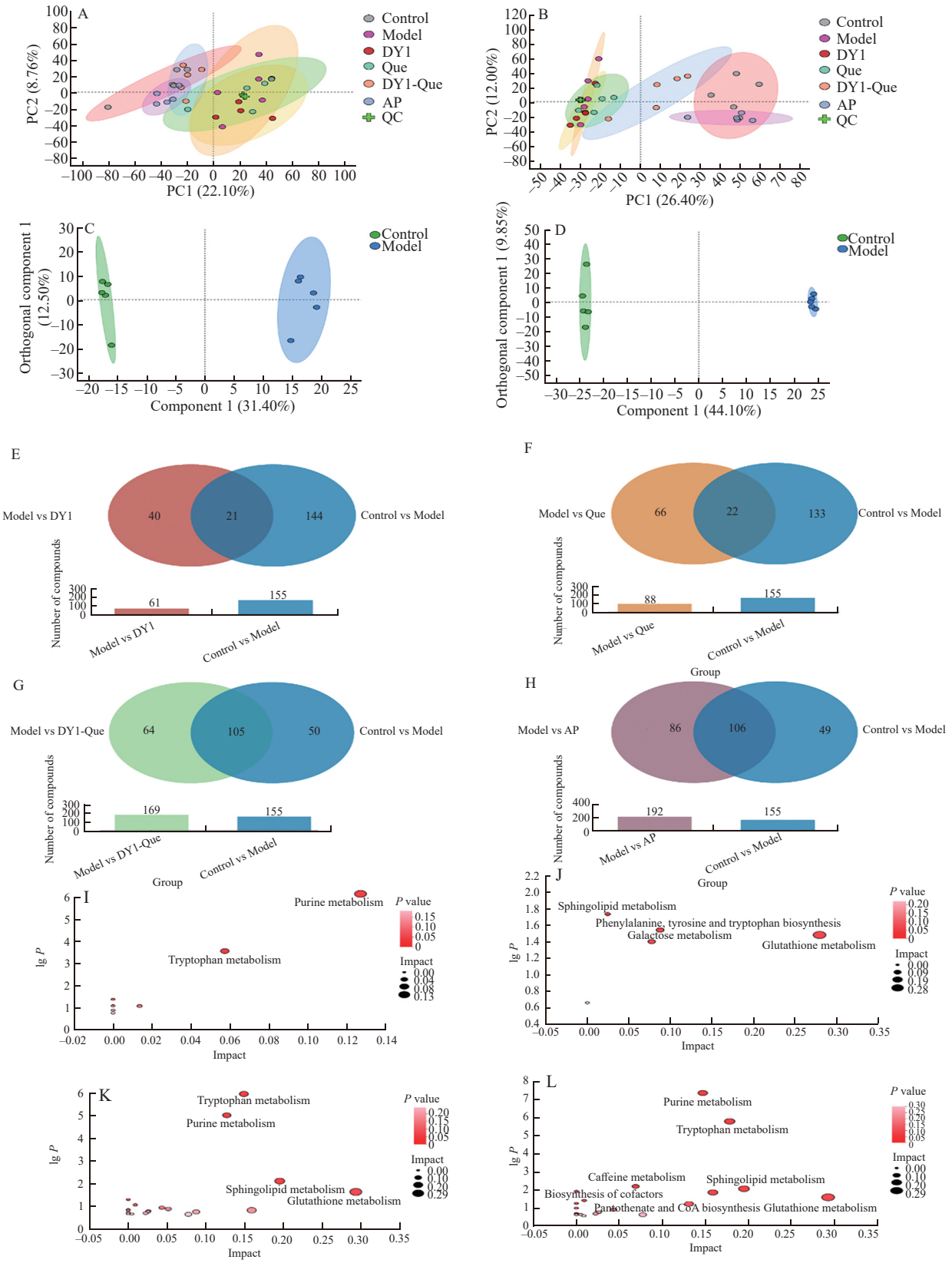

Fig. 5 Metabolic profiling and KEGG topological analysis bubble map. (A) PCA score diagram (cation). (B) PCA score diagram (anion). (C) OPLS-DA score plot in positive. (D) OPLS-DA score plot in negative. Venn diagrams of Control vs Model and Model vs DY1 (E), Control vs Model and Model vs Que (F), Control vs Model and Model vs DY1-Que (G), Control vs Model and Model vs AP (H). Pathway enrichment analysis of Model vs Control and DY1 vs Model (I), Model vs Control and Que vs Model (J), Model vs Control and DY1-Que vs Model (K), Model vs Control and AP vs Model (L). $n = 5$ per group.

biosynthesis of cofactors (impact > 0, $P < 0.05$). Overall, our metabolomics analysis revealed that the intervention by *L. plantarum* DY1 and quercetin influenced various metabolic pathways associated with HUA. DY1-Que significantly regulated four metabolic pathways, while DY1 and Que regulated two metabolic pathways, respectively. The effect of DY1-Que on the regulation of metabolic disorders was stronger than that of DY1 and Que, indicating that *L. plantarum* DY1 and quercetin had a synergistic effect on the alleviation of HUA.

3.9 Correlation analysis

The alterations in the gut microbiota exhibited a strong association with changes observed in the serum metabolic profile. Correlation analysis revealed that *Lactobacillus*, norank_f__norank_o__Clostridia_UCG-014, and *Roseburia* were significantly associated with 15 biomarkers (Fig. S11). *Lactobacillus* demonstrated a negative correlation with glutathione, oxidized glutathione, sphingonine, 3-methylindole, UA, and xanthosine, cAMP, AMP, and ADP levels, and a positive correlation with indole-3-acetamide.

The norank_f__norank_o__Clostridia_UCG-014 was significantly negatively correlated with 5-hydroxy-*L*-tryptophan and indole-3-acetamide levels, and positively correlated with 3-methylindole and so on. Similarly, we found that *Roseburia* was significantly associated with 13 biomarkers. These findings highlighted the complex interactions between metabolites and the gut microbiome, which influenced each other's composition and function. It also suggested that the regulation of the abundance of three bacteria by probiotics and quercetin might potentially participate in glutathione metabolism, sphingolipid metabolism, purine metabolism, and tryptophan metabolism.

3.10 FMT has the potential to enhance HUA

After a seven-day course of antibiotic treatment, the abundance of OTUs in the intestinal microbiota of antibiotic-treated mice exhibited a significant reduction compared to that of normal mice, thereby confirming the successful establishment of an aseptic mouse model (Fig. S12). To further elucidate the functional role of gut microbiota, we conducted FMT experiments as depicted in Figs. 6A-B. The transfer of fecal microbiota from donors treated with *L. plantarum* DY1 and quercetin to antibiotic treated hosts resulted in a notable decrease in serum UA levels among the DY1-Que (FMT) group. Subsequent analysis revealed that post-treatment gut microbial composition was

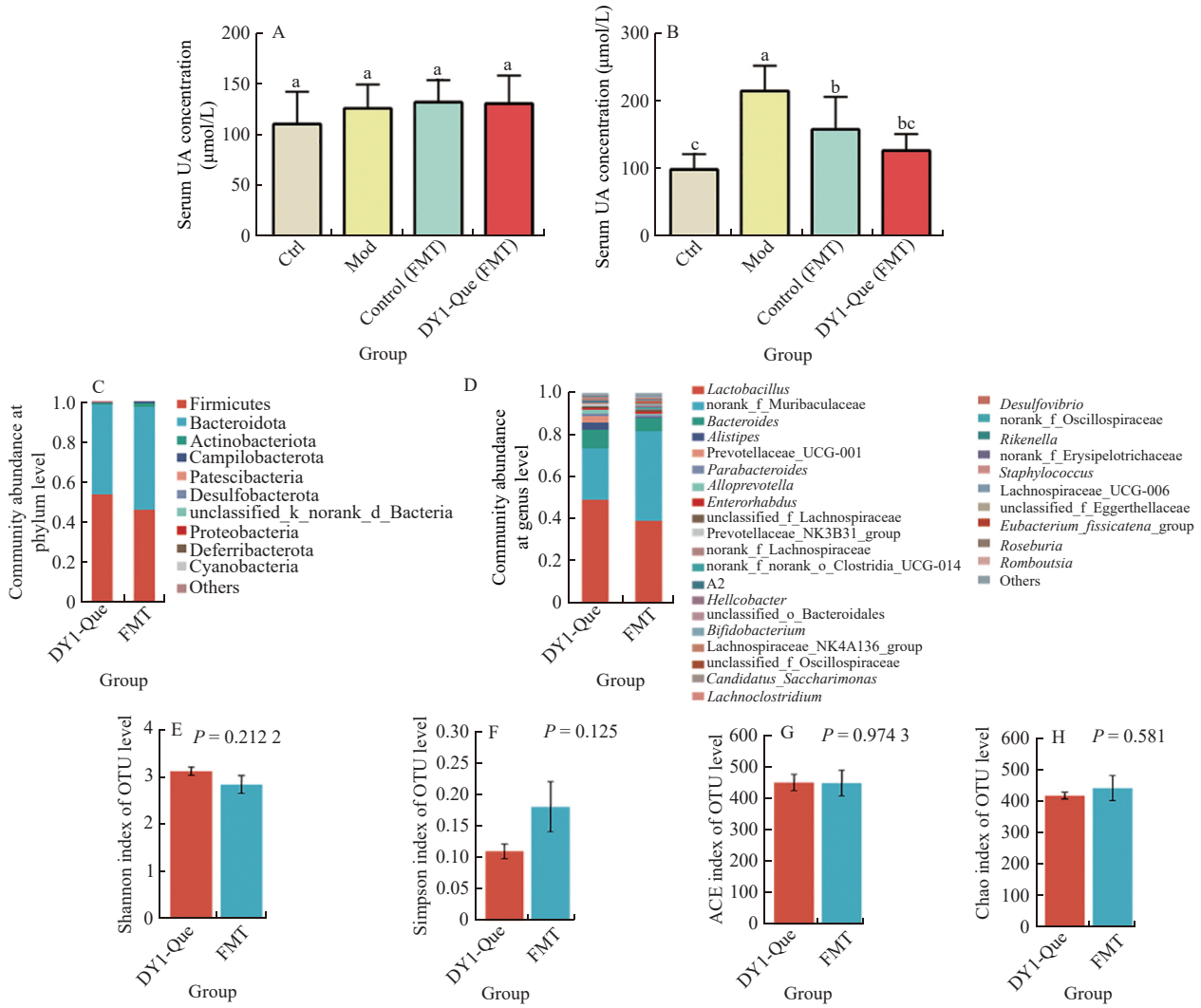

Fig. 6 Serum UA concentration in 0 day (A), 35 days (B). Bar chart of relative abundance at phylum level (C), genus level (D). (E) Shannon index. (F) Simpson index. (G) ACE index. (H) Chao index. Values with different letters represent significant differences ($P < 0.05$). (A-B) $n = 8$ per group; (C-H) $n = 5$ per group.

successfully established in HUA mice through FMT procedures. At the phylum level, taxonomic analysis revealed a high degree of similarity between the microbial communities of FMT recipient mice and those of donor mice. No significant alteration in α-diversity was observed when comparing donor and FMT recipient mice. The horizontal histogram of genus distribution showed that *Lactobacillus*, norank_f__norank_o__Clostridia_UCG-014, and *Roseburia* were detected in the feces of mice undergoing FMT. These findings provide evidence for successful transplantation of gut microbiota in HUA mice following administration (Figs. 6C-H). Furthermore, FMT results demonstrate that the combined administration of *L. plantarum* DY1 and quercetin effectively mitigates HUA through modulation of the gut microbiota.

4. Discussion

UA represents the ultimate end product of purine metabolism, with approximately 80% being synthesized through bodily purine metabolic pathways. HUA mice exhibited enhanced serum XOD and ADA activity in the liver compared to healthy mice. ADA facilitates the conversion of adenine nucleoside derived from adenine nucleotides breakdown into hypoxanthine nucleoside, subsequently leading to the production of UA through XOD catalytic oxidation[18]. Recent studies have revealed that certain probiotics, particularly *Lactobacillus* strains, possess the capability to enzymatically degrade UA, purine, and nucleosides. *Limosilactobacillus ferum* jl-3 has been demonstrated to effectively degrade UA *in vivo*. We isolated a unique strain of LAB, specifically *L. plantarum* DY1, which exhibited superior degradation capabilities for UA (93.97%), purine (87.98%), and nucleoside (100%). *L. plantarum* DY1 effectively suppressed the activity of XOD, resulting in a significant reduction in UA production. This strain exhibited an impressive inhibition rate of 40.3% towards XOD, which aligns with recent studies indicating *L. fermentum* NCUH003018 exhibiting an XOD inhibition rate of 20.87%[19].

Hydrophobicity is a crucial characteristic of probiotics that necessitates consideration during the screening process for potential probiotics. Moreover, a high level of aggregation ability can effectively hinder the colonization of pathogenic bacteria in the gastrointestinal tract of the host. Fortunately, DY1 demonstrates exceptional hydrophobicity and aggregation capacity.

Flavonoids compounds were the main active components of many natural plants. They had broad-spectrum pharmacological activities and low toxicity, such as antioxidant, anti-atherosclerosis, anti-hypertension, hypoglycemic, anti-inflammatory, antibacterial, antiviral, anticancer, etc. They were important resources for food functional factors and new drug research and development. Quercetin, as a flavonoids compound, had certain UA inhibition ability[20]. To date, most investigations on reducing serum UA levels have primarily focused on the utilization of probiotics or individual natural foodborne compounds; however, limited findings exist regarding synbiotics. Therefore, based on the screening of probiotics with a potential lowering UA effect, investigate the synergistic therapeutic effect of probiotics and prebiotics on HUA.

HUA can lead to kidney and liver injury as well as increase the levels of inflammatory factors[21]. In the present study, *L. plantarum* DY1 demonstrated a synergistic reduction in serum UA levels when combined with quercetin. This combination also exhibited a protective effect against HUA-induced liver and kidney damage while mitigating inflammation by reducing the levels of kidney inflammatory factors. Notably, allopurinol, a commonly used medication for HUA, may have the potential to exacerbate kidney damage. The transporters involved in urate reabsorption encompass GLUT9 and URAT1, whereas those implicated in urate excretion comprise OAT1, ABCG2, and other potential transporters[22]. The potential mechanism underlying the regulation of urate excretion may be attributed to the predominant influence on relevant transport genes. Specifically, the expression of the UA reabsorption transporter gene was suppressed, resulting in a reduction in kidney absorption of UA or increasing the excretion of UA by the kidneys by promoting the expression of the gene for UA excretion. For example, *L. rhamnosus* LR1155 and *L. ferment* LF2644 were found to up-regulate the expression of urate transporter genes as well as the *ABCG2* gene in colon and jejunum tissues[23]. Our results demonstrate that combination treatment with *L. plantarum* DY1 and quercetin effectively reversed the mRNA expression of *URAT1*, *GLUT9*, *OAT1*, and *ABCG2*.

The balance of the gut microbiota in the host organism is closely linked to the overall health of the host, especially in relation to metabolic syndrome. Imbalance of the gut microbiota can significantly impact the development of HUA[24]. Yang et al.[25] discovered that the α-diversity index of intestinal flora in HUA patients was higher compared to healthy controls, found a result similar to our study. Firmicutes and Bacteroidetes constitute over 90% of the intestinal tract, while Actinomyces, as one of the four major phyla in the gut microbiome, plays a crucial role in maintaining gut homeostasis despite its relatively small proportion. Multiple studies have shown that HUA results in an unbalanced ratio of Firmicutes to Bacteroidetes and a decrease in the abundance of Actinomycetes. Supplementation with probiotics or prebiotics can improve this imbalance and thus achieve the goal of treating HUA[26-27]. In this study, the administration of *L. plantarum* DY1 and quercetin improved the imbalance between Firmicutes and Bacteroidetes and increased the abundance of Actinomycetes. *Lactobacillus* is a key member of the gut microbiome, metabolizing carbohydrates, secreting short-chain fatty acids, and reducing inflammation in mice. The abundance of *Lactobacillus* increased to different extents after combined treatment with *L. plantarum* DY1 and quercetin. Although there was evidence of an augmented abundance of *Roseburia* in the gut microbiota of rats with HUA[28], the individual administration of *L. plantarum* DY1 or quercetin alone exhibited a mitigating effect on the increased abundance of *Roseburia*, while the combined treatment resulted in the most significant reduction in relative abundance. These findings suggest the combined treatment synergistically modulates the composition and structure of intestinal microbes, leading to an alleviation of UA levels. Notably, they promote the proliferation of beneficial microbial populations such as *Lactobacillus*, while concurrently inhibiting detrimental bacterial growth like that observed for *Roseburia.*

Probiotics and quercetin have been identified as key players in distinct metabolic pathways, with their synergistic action effectively modulating glutathione metabolism, sphingolipid metabolism, purine metabolism, and tryptophan metabolism.

Glutathione has an effect on oxidative stress and inflammation, both of which play a key role in the pathogenesis of HUA[29]. Sphingolipids play crucial roles in various physiological functions and are involved in a wide range of intricate metabolic processes, particularly those related to HUA[30-31]. Tryptophan metabolism primarily encompasses three pathways: the kynurenine pathway, the serotonin/5-hydroxytryptamine (5-HT) pathway, and the indole pathway. Tryptophan and its metabolites exert bidirectional effects on

the gut microbiota through signaling mechanisms involving immunity and metabolism, ultimately influencing host organism function. Previous investigations have demonstrated a close association between tryptophan and its related metabolites and HUA[32]. Our study revealed that the combined action of *L. plantarum* DY1 and quercetin synergistically reduced the levels of indoleacetaldehyde, 3-(3-indolyl)-2-oxopropanoic acid, 3-indoleacetic acid, and 3-methylindole in HUA mice while concurrently upregulating the levels of indole-3-acetamide and 5-hydroxy-*L*-tryptophan. 3-Indoleacetic acid is synthesized through the catabolic pathway of tryptophan, and its pro-oxidative and pro-inflammatory characteristics may lead to glomerular sclerosis and renal interstitial fibrosis. This indole-derived toxin demonstrates nephrotoxic effects *in vivo*[33]. 5-HT serves as a pivotal gastrointestinal signaling molecule that mediates communication between endogenous or exogenous neurons within the intestines. It profoundly influences intestinal peristalsis, movement coordination, secretion regulation, blood vessel dilation dynamics, and nutrient absorption processes. The synthesis of 5-HT relies on the precursor compound known as 5-hydroxy-*L*-tryptophan. It is noteworthy that the gut microbiota significantly modulates this serotonin pathway's production. By regulating intestinal motility and immunity responses within the gut environment itself, 5-HT impacts microbial composition[34]. Moreover, indole-3-acetamide produced by *Lactobacillus* could reduce liver damage as a tryptophan metabolite, similar to our study. The correlation analysis between gut microbiota and serum metabolites also confirmed the result. *Lactobacillus* had a strong positive correlation with indole-3-acetamide, while norank_ f_norank_o_Clostridia_UCG-014 and *Roseburia* were significantly negatively correlated with indole-3-acetamide. Therefore, the combination of *L. plantarum* and quercetin might regulate tryptophan biosynthesis by maintaining gut microbiota stability.

Purines play crucial roles in nucleic acid synthesis and energy conversion reactions, which are essential for maintaining the normal physiological function of cells. In the process of phosphoric acid phosphoribosyl pyrophosphate (PRPP) synthase catalysis, 5-phosphate ribose and adenosine triphosphate (ATP) form PRPP. Subsequently, PRPP undergoes a series of reactions to generate inosine monophosphate (IMP). IMP interacts with AMP and guanosine monophosphate (GMP). AMP is converted to adenosine by the action of 5' nucleotidase (5'NT), followed by its transformation into inosine through ADA. GMP is enzymatically converted into guanosine, which is subsequently transformed into guanine by the action of purine nucleotide phosphorylase (PNP). Guanine undergoes further oxidation to form xanthine. IMP can be metabolized to inosine via 5'NT, hypoxanthine through PNP, or directly converted to hypoxanthine by hypoxanthine guanine phosphoribose transferase and PRPP. Hypoxanthine is then oxidized into xanthine by the enzyme XOD, ultimately leading to the production of UA[35]. In this study, significant reductions in the levels of UA, xanthosine, cAMP, ADP, and AMP were observed following the combination treatment of *L. plantarum* DY1 and quercetin, which might indicate inhibition of XOD activity. This was consistent with the current findings. Correlation analysis also confirmed that these purine metabolites were significantly negatively correlated with *Lactobacillus* and negatively correlated with norank_ f_norank_o_Clostridia_UCG-014 and *Roseburia*. Therefore, we suggest that the improvement of gut microbiota imbalance and the change of differential metabolites in mice with HUA induced by combination therapy are the driving factors of its uric-lowering effect.

With the shift from correlational research to machine-assisted investigation in microbiota studies, specific microbiota and their byproducts have been employed in the examination of diseases such as metabolic syndrome. By introducing the microbial community from a healthy donor's gut or feces into the gastrointestinal tract of the recipient, it can rapidly modify the recipient's gut microbiota and replicate certain attributes of the donor[36]. Zhang et al.[37] found that not only oral administration of bitter melon could reduce blood lipids, but transplantation of donor bitter melon to treat the gut microbiota of mice also alleviated hyperlipidemia. Our first study revealed that the combined action of *L. plantarum* DY1 and quercetin effectively alleviates UA levels by modulating the gut microbiota. To establish a nearly bacteria-free mouse model, we employed an antibiotic cocktail therapy followed by FMT from donor mice to HUA mice. As anticipated, FMT exhibited therapeutic effects in reducing HUA and successfully regulating gut microbiota in these mice. These findings not only underscore the significance of gut microbiota but also provide evidence for the regulatory effects of synbiotics on gut microbiota, thereby further supporting our conclusions.

5. Conclusion

In conclusion, the combination of *L. plantarum* DY1 and quercetin exhibited superior anti-HUA effects compared to the individual effects of *L. plantarum* DY1 or quercetin alone. This effect was observed through multiple targets, including inhibition of XOD and ADA activity, absorption or degradation of UA, purine, and nucleoside compounds, reduction in inflammatory factor levels, modulation of urate transporter gene expression, as well as involvement in the increases in abundance of *Lactobacillus* and the decreases in abundance of norank_f_norank_o_Clostridia_UCG-014 and *Roseburia*, which restored the composition of intestinal flora. This combination favorably regulates metabolic disorders involved in glutathione metabolism (oxidized glutathione, glutathione), sphingolipid metabolism (sphingosine, sphinganine), purine metabolism (UA, xanthosine, cAMP, ADP, and AMP), and tryptophan metabolism (indoleacetaldehyde, 3-methylindole, 3-(3-indolyl)-2-oxopropanoic acid, indole-3-acetamide, 5-hydroxy-*L*-tryptophan, and 3-indoleacetic acid), Meanwhile, FMT further indicated the crucial role of the gut microbiota in adjusting the body's metabolic network for the formation and elimination of UA.

Conflict of interest

The authors declare no conflicts of interest.

Acknowledgements

This work was supported by National Science and Technology Fundamental Resources Investigation Program of China (2019FY100700).

Appendix A. Supplementary information

Supplementary data associated with this article can be found, in the online version, at http://doi.org/10.26599/FSHW.2024.9250264.

References

[1] M. Drabkin, Y. Yogev, L. Zeller, et al., Hyperuricemia and gout caused by missense mutation in *D*-lactate dehydrogenase, J. Clin. Invest. 129 (2019) 5163-5168. https://doi.org/10.1172/jci129057.

[2] S.W. Jung, S. Kim, Y.G. Kim, et al., Uric acid and inflammation in kidney disease, Am. J. Physiol. Renal. Physiol. 318 (2020) 1327-1340. https://doi.org/10.1152/ajprenal.00272.2019.

[3] Y. Chen, L.Y. Luo, S.S. Hu, et al., The chemistry, processing, and preclinical anti-hyperuricemia potential of tea: a comprehensive review, Crit. Rev. Food Sci. Nutr. 63 (2023) 7065-7090. https://doi.org/10.1080/10408398.2022.2040417.

[4] M. Furuhashi, New insights into purine metabolism in metabolic diseases: role of xanthine oxidoreductase activity, Am. J. Physiol. Endocrinol. Metab. 319 (2020) E827-E834. https://doi.org/10.1152/ajpendo.00378.2020.

[5] Z.H. Qu, P.J. Tian, B. Yang, et al., Fecal microbiota transplantation for diseases: therapeutic potential, methodology, risk management in clinical practice, Life Sci. 304 (2022) 120719. https://doi.org/10.1016/j.lfs.2022.120719.

[6] Y.T. Tung, C.A. Hsu, C.S. Chen, et al., Phytochemicals from acacia confusa heartwood extracts reduce serum uric acid levels in oxonate-induced mice: their potential use as xanthine oxidase inhibitors, J. Agric. Food Chem. 58 (2010) 9936-9941. https://doi.org/10.1021/jf102689k.

[7] R. Martín, F. Chain, S. Miquel, et al., Using murine colitis models to analyze probiotics-host interactions, FEMS Microbiol. Rev. 41 (2017) S49-S70. https://doi.org/10.1093/femsre/fux035.

[8] T.L. Shi, X.Y. Bian, Z.X. Yao, et al., Quercetin improves gut dysbiosis in antibiotic-treated mice, Food Funct. 11 (2020) 8003-8013. https://doi.org/10.1039/d0fo01439g.

[9] Q.H. Hu, X. Zhang, X. Wang, et al., Quercetin regulates organic ion transporter and uromodulin expression and improves renal function in hyperuricemic mice, Eur. J. Nutr. 51 (2012) 593-606. https://doi.org/10.1007/s00394-011-0243-y.

[10] Z.J. Liu, F. Liu, W. Wang, et al. Study of the alleviation effects of a combination of *Lactobacillus rhamnosus* and inulin on mice with colitis, Food Funct. 11 (2020) 3823-3837. https://doi.org/10.1039/c9fo02992c.

[11] Y. Wu, Z. Ye, P.Y. Feng, et al., *Limosilactobacillus fermentum* jl-3 isolated from "jiangshui" ameliorates hyperuricemia by degrading uric acid, Gut Microbes. 13 (2021) 1-18. https://doi.org/10.1080/19490976.2021.1897211.

[12] J.X. Lin, T. Xiong, Z. Peng., et al., Novel lactic acid bacteria with anti-hyperuricemia ability: screening and *in vitro* probiotic characteristics, Food Biosci. 49 (2022) 101840. https://doi.org/10.1016/j.fbio.2022.101840.

[13] M.V. Niederle, J. Bosch, C.E. Ale, et al., Skin-associated lactic acid bacteria from North American bullfrogs as potential control agents of *Batrachochytrium dendrobatidis*, PLoS ONE 14 (2019) e223020. https://doi.org/10.1371/journal.pone.0223020.

[14] S. Rodríguez-Sánchez, P. Fernández-Pacheco, S. Seseña, et al., Selection of probiotic *Lactobacillus* strains with antimicrobial activity to be used as biocontrol agents in food industry, LWT-Food Sci. Technol. 143 (2021) 111142. https://doi.org/10.1016/j.lwt.2021.111142.

[15] M. Umamaheswari, K. Asokkumar, A. Somasundaram, et al., Xanthine oxidase inhibitory activity of some indian medical plants, J. Ethnopharmacol. 109 (2007) 547-551. https://doi.org/10.1016/j.jep.2006.08.020.

[16] T.Q. Yong, D.L. Liang, S.D Chen, et al., Caffeic acid phenethyl ester alleviated hypouricemia in hyperuricemic mice through inhibiting XOD and up-regulating OAT3, Phytomedicine 103 (2022) 154256. https://doi.org/10.1016/j.phymed.2022.154256.

[17] X.F. Zhou, B.W. Zhang, X.L. Zhao, et al., Chlorogenic acid supplementation ameliorates hyperuricemia, relieves renal inflammation, and modulates intestinal homeostasis, Food Funct. 12 (2021) 5637-5649. https://doi.org/10.1039/d0fo03199b.

[18] Y.Z. Le, X. Zhou, J.W. Zheng, et al., Anti-hyperuricemic effects of astaxanthin by regulating xanthine oxidase, adenosine deaminase and urate transporters in rats, Mar. Drugs 18 (2020) 610. https://doi.org/10.3390/md18120610.

[19] X.T. Zhao, F. Peng, Z.G. Liu, et al., Lactic acid bacteria with anti-hyperuricemia ability: screening *in vitro* and evaluating in mice, Food Biosci. 52 (2023) 102411. https://doi.org/10.1016/j.fbio.2023.102411.

[20] T. Nutmakul, A review on benefits of quercetin in hyperuricemia and gouty arthritis, Saudi Pharm. J. 30 (2022) 918-926. https://doi.org/10.1016/j.jsps.2022.04.013.

[21] L.J. Liu, S.J. Jiang, X.Q. Liu, et al., Inflammatory response and oxidative stress as mechanism of reducing hyperuricemia of *Gardenia jasminoides-Poria cocos* with network pharmacology, Oxid. Med. Cell Longev. 2021 (2021) 1-18. https://doi.org/10.1155/2021/8031319.

[22] Z.Z. Qin, S.B. Wang, Y.H. Lin, et al., Antihyperuricemic effect of mangiferin aglycon derivative J99745 by inhibiting xanthine oxidase activity and urate transporter 1 expression in mice, Acta Pharm. Sin. B. 8 (2018) 306-315. https://doi.org/10.1016/j.apsb.2017.05.004.

[23] Y.J. Li, J. Zhu, G.D. Lin, et al., Probiotic effects of *Lacticaseibacillus rhamnosus* 1155 and *Limosilactobacillus fermentum* 2644 on hyperuricemic rats, Front. Nutr. 9 (2022) 993951. https://doi.org/10.3389/fnut.2022.993951

[24] B.M. Tian, Y. Geng, P.Y. Wang, et al., Ferulic acid improves intestinal barrier function through altering gut microbiota composition in high-fat diet-induced mice, Eur. J. Nutr. 61 (2022) 3767-3783. https://doi.org/10.1007/s00394-022-02927-7.

[25] H.T. Yang, W.J. Xiu, J.K. Liu, et al., Gut microbiota characterization in patients with asymptomatic hyperuricemia: probiotics increased, Bioengineered. 12 (2021) 7263-7275. https://doi.org/10.1080/21655979.2021.1976897.

[26] F.E. García-Arroyo, G. Gonzaga, I. Muñoz-Jiménez, et al., Probiotic supplements prevented oxonic acid-induced hyperuricemia and renal damage, PLoS ONE 13 (2018) e202901. https://doi.org/10.1371/journal.pone.0202901.

[27] H.T. Wan, J.J. Han, S.S. Tang, et al., Comparisons of protective effects between two sea cucumber hydrolysates against diet induced hyperuricemia and renal inflammation in mice, Food Funct. 11 (2020) 174-186. https://doi.org/10.1039/c9fo02425e.

[28] N.H. Zhang, J.X. Zhou, L. Zhao, et al., Ferulic acid supplementation alleviates hyperuricemia in high-fructose/fat diet-fed rats via promoting uric acid excretion and mediating the gut microbiota, Food Funct. 14 (2023) 1710-1725. https://doi.org/10.1039/d2fo03332a.

[29] M.W. Wang, J. Zhao, N. Zhang, et al., Astilbin improves potassium oxonate-induced hyperuricemia and kidney injury through regulating oxidative stress and inflammation response in mice, Biomed. Pharmacother. 83 (2016) 975-988. https://doi.org/10.1016/j.biopha.2016.07.025.

[30] N.Q. Qin, Y. Jiang, W.J. Shi, et al., High-throughput untargeted serum metabolomics analysis of hyperuricemia patients by UPLC-Q-TOF/MS, Evid. Based Complement Alternat. Med. 2021 (2021) 1-15. https://doi.org/10.1155/2021/5524772.

[31] G. Norris, C. Blesso. Dietary and endogenous sphingolipid metabolism in chronic inflammation, Nutrients 9 (2017) 1180. https://doi.org/10.3390/nu9111180.

[32] B.X. Shan, T. Chen, B.X. Huang, et al., Untargeted metabolomics reveal the therapeutic effects of Ermiao Wan categorized formulas on rats with hyperuricemia, J. Ethnopharmacol. 281 (2021) 114545. https://doi.org/10.1016/j.jep.2021.114545.

[33] R. Vial, S. Poitevin, N. Mckay, et al., Tryptophan metabolites regulate neuropentraxin 1 expression in endothelial cells, Int. J. Mol. Sci. 23 (2022) 2369. https://doi.org/10.3390/ijms23042369.

[34] N. Liu, S.Q. Sun, P.J. Wang, et al., The mechanism of secretion and metabolism of gut-derived 5-hydroxytryptamine, Int. J. Mol. Sci. 22 (2021) 7931. https://doi.org/10.3390/ijms22157931.

[35] Z. Huang, N. Xie, P. Illes, et al., From purines to purinergic signaling: molecular functions and human diseases, Signal. Transduct. Target Ther. 6 (2021) 162. https://doi.org/10.1038/s41392-021-00553-z.

[36] B.T. Cui, P. Li, L.J. Xu, et al., Step-up fecal microbiota transplantation (FMT) strategy, Gut Microbes. 7 (2016) 323-328. https://doi.org/10.1080/19490976.2016.1151608.

[37] F. Zhang, X.P. Zhang, J.Q. Yu, et al., The gut microbiota confers the lipid-lowering effect of bitter melon (*Momordica charantia* L.) in high-fat diet (HFD) -induced hyperlipidemic mice, Biomed. Pharmacother. 131 (2020) 110667. https://doi.org/10.1016/j.biopha.2020.110667.